Kinetic, Stereochemical, and Structural Effects of Mutations of the Active Site Arginine Residues in 4-Oxalocrotonate Tautomerase †

9 AUTHORS, INCLUDING:

Robert Czerwinski
PELOTON THERAPEUTICS, INC.
33 PUBLICATIONS **941** CITATIONS

SEE PROFILE

Patricia Legler
United States Naval Research Laboratory
40 PUBLICATIONS **527** CITATIONS

SEE PROFILE

Kinetic, Stereochemical, and Structural Effects of Mutations of the Active Site Arginine Residues in 4-Oxalocrotonate Tautomerase[†]

Thomas K. Harris,[‡,§] Robert M. Czerwinski,[§,‖] William H. Johnson, Jr.,[‖] Patricia M. Legler,[‡]
Chitrananda Abeygunawardana,[‡] Michael A. Massiah,[‡] James T. Stivers,[‡] Christian P. Whitman,*,[‖] and
Albert S. Mildvan*,[‡]

*Department of Biological Chemistry, The Johns Hopkins School of Medicine, 725 North Wolfe Street,
Baltimore, Maryland 21205-2185, and Medicinal Chemistry Division, College of Pharmacy, The University of Texas,
Austin, Texas 78712-1074*

Received May 14, 1999; Revised Manuscript Received July 2, 1999

ABSTRACT: Three arginine residues (Arg-11, Arg-39, Arg-61) are found at the active site of 4-oxalocrotonate tautomerase in the X-ray structure of the affinity-labeled enzyme [Taylor, A. B., Czerwinski, R. M., Johnson, R. M., Jr., Whitman, C. P., and Hackert, M. L. (1998) *Biochemistry 37*, 14692−14700]. The catalytic roles of these arginines were examined by mutagenesis, kinetic, and heteronuclear NMR studies. With a 1,6-dicarboxylate substrate (2-hydroxymuconate), the R61A mutation showed no kinetic effects, while the R11A mutation decreased k_{cat} 88-fold and increased K_m 8.6-fold, suggesting both binding and catalytic roles for Arg-11. With a 1-monocarboxylate substrate (2-hydroxy-2,4-pentadienoate), no kinetic effects of the R11A mutation were found, indicating that Arg-11 interacts with the 6-carboxylate of the substrate. The stereoselectivity of the R11A-catalyzed protonation at C-5 of the dicarboxylate substrate decreased, while the stereoselectivity of protonation at C-3 of the monocarboxylate substrate increased in comparison with wild-type 4-OT, indicating the importance of Arg-11 in properly orienting the dicarboxylate substrate by interacting with the charged 6-carboxylate group. With 2-hydroxymuconate, the R39A and R39Q mutations decreased k_{cat} by 125- and 389-fold and increased K_m by 1.5- and 2.6-fold, respectively, suggesting a largely catalytic role for Arg-39. The activity of the R11A/R39A double mutant was at least 10^4-fold lower than that of the wild-type enzyme, indicating approximate additivity of the effects of the two arginine mutants on k_{cat}. For both R11A and R39Q, 2D $^1H-^{15}N$ HSQC and 3D $^1H-^{15}N$ NOESY−HSQC spectra showed chemical shift changes mainly near the mutated residues, indicating otherwise intact protein structures. The changes in the R39Q mutant were mainly in the β-hairpin from residues 50 to 57 which covers the active site. HSQC titration of R11A with the substrate analogue *cis,cis*-muconate yielded a K_d of 22 mM, 37-fold greater than the K_d found with wild-type 4-OT (0.6 mM). With the R39Q mutant, *cis,cis*-muconate showed negative cooperativity in active site binding with two K_d values, 3.5 and 29 mM. This observation together with the low K_m of 2-hydroxymuconate (0.47 mM) suggests that only the tight binding sites function catalytically in the R39Q mutant. The $^{15}N\epsilon$ resonances of all six Arg residues of 4-OT were assigned, and the assignments of Arg-11, -39, and -61 were confirmed by mutagenesis. The binding of *cis,cis*-muconate to wild-type 4-OT upshifts Arg-11 Nϵ (by 0.05 ppm) and downshifts Arg-39 Nϵ (by 1.19 ppm), indicating differing electronic delocalizations in the guanidinium groups. A mechanism is proposed in which Arg-11 interacts with the 6-carboxylate of the substrate to facilitate both substrate binding and catalysis and Arg-39 interacts with the 1-carboxylate and the 2-keto group of the substrate to promote carbonyl polarization and catalysis, while Pro-1 transfers protons from C-3 to C-5. This mechanism, together with the effects of mutations of catalytic residues on k_{cat}, provides a quantitative explanation of the 10^7-fold catalytic power of 4-OT. Despite its presence in the active site in the crystal structure of the affinity-labeled enzyme, Arg-61 does not play a significant role in either substrate binding or catalysis.

4-Oxalocrotonate tautomerase (4-OT,[1] EC 5.3.2), an enzyme elaborated by the soil bacterium *Pseudomonas putida mt-2*, catalyzes the isomerization of unconjugated α-keto acids such as 2-oxo-4-hexenedioate (**1**) to its conjugated isomer 2-oxo-3-hexenedioate (**3**) through the dienol intermediate 2-hydroxy-2,4-hexadienedioate (**2**) known more commonly as 2-hydroxymuconate (Scheme 1) (*1*). The enzyme is part of a degradative pathway that converts various
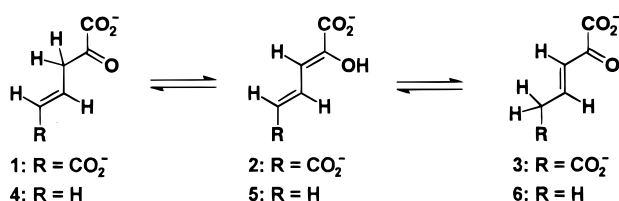
* Address correspondence to either author. C.P.W.: tel, 512-471-6198; fax, 512-232-2606; e-mail, cwhitman@uts.cc.utexas.edu. A.S.M.: tel, 410-955-2038; fax, 410-955-5759; e-mail, mildvan@welchlink.welch.jhu.edu.

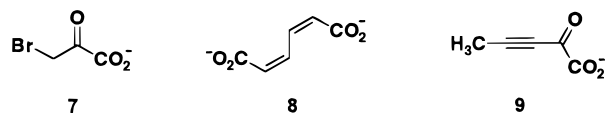[‡] The Johns Hopkins School of Medicine.

[§] These authors contributed equally to this work.

[‖] The University of Texas at Austin.

Scheme 1

1: R = CO2−
4: R = H

2: R = CO2−
5: R = H

3: R = CO2−
6: R = H

Scheme 2

7   8   9

aromatic hydrocarbons to intermediates in the Krebs cycle (*2*). A large body of evidence has been obtained demonstrating that 4-OT catalyzes a suprafacial 1,3-allylic rearrangement, which is mediated by a single base identified as the amino-terminal proline (*3−10*).

In addition to Pro-1, a number of other active site residues have been identified, and potential roles in catalysis have been suggested for them. It was anticipated that the 4-OT-catalyzed reaction would involve a general acid catalyst as well as the general base catalyst because general acid−base catalysis is used in analogous keto−enol tautomerizations catalyzed by triosephosphate isomerase (*11−13*) and ketosteroid isomerase (*14−16*). A crystal structure of an isozyme of 4-OT, solved in the absence of a ligand, first suggested that Arg-39 might be the general acid catalyst as well as the residue responsible for binding the C-1 carboxylate group of the substrate (*4*). Subsequent NMR studies supported this role for Arg-39 by demonstrating that covalent binding of the monocarboxylate affinity label 3-bromopyruvate (**7**, Scheme 2) to the enzyme resulted in changes in the backbone amide chemical shifts of Arg-39 only, while binding of the dicarboxylate competitive inhibitor *cis,cis*-muconate (**8**, CCM, Scheme 2) to the enzyme caused changes in the backbone amide chemical shifts of both Arg-39 and another residue, Arg-11 (*8*). Arg-11 had previously been suggested by the crystal structure as the residue responsible for the binding of the substrate C-6 carboxylate group (*4*). In addition to their direct involvement in the mechanism, it was suggested that the electrostatic effects of Arg-11 and Arg-39 might contribute to lowering the pK_a of Pro-1 to 6.4 (*6*).

A recent 2.4 Å crystal structure of 4-OT inactivated by the active site-directed irreversible inhibitor 2-oxo-3-pentynoate (**9**, Scheme 2) provided further insight into the catalytic role of Arg-39 and also found Arg-61 and an ordered water molecule to be in the active site (Figure 1A) (*17*). Examination of the inactivated enzyme complex shows the side chain ϵ-nitrogen of Arg-39 to be 2.9 Å from the
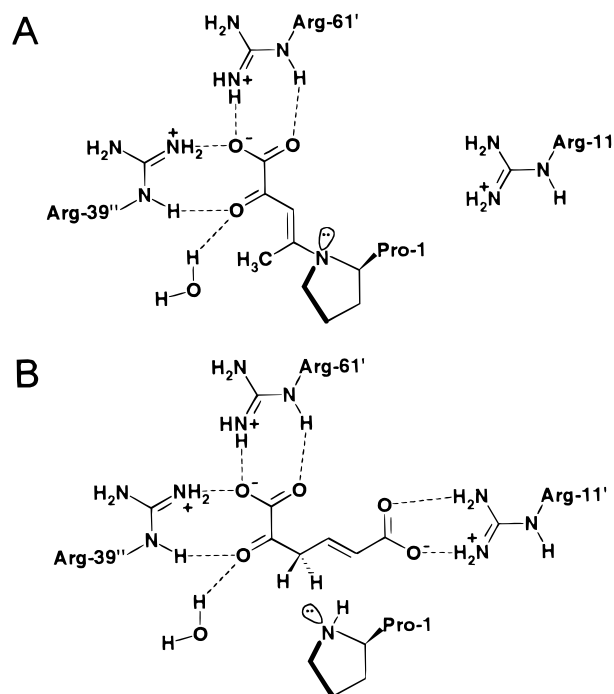
FIGURE 1: (A) Active site region of 4-OT from the X-ray structure of the enzyme inactivated by the mechanism-based inhibitor 2-oxo-3-pentynoate (*17*). (B) Presumed mode of binding of the substrate 2-oxo-4-hexenedioate based on the structure in panel A and NMR studies (*7, 8*). The primed residues come from other subunits.

C-2 carbonyl oxygen of the adduct while the η-nitrogen is 2.7 Å from a C-1 carboxylate oxygen (*17*). The ordered water molecule may also interact with the carbonyl oxygen at a distance of 3.2 Å (*17*). Arg-61 appears to interact with the C-1 carboxylate group in a bidentate fashion: the side chain η-nitrogen is 3.2 Å from one carboxylate oxygen and the ϵ-nitrogen is 3.0 Å from the other carboxylate oxygen. These observations suggested a working hypothesis for the binding of the substrate **1**, which is depicted in Figure 1B (*17*). However, since uncertainties in interatomic distances in protein crystal structures are at least 0.1 times the resolution (*18*), which in the present case would be ≥±0.24 Å, it is not clear which hydrogen bonds in Figure 1 actually form and whether they contribute to catalysis. Moreover, the structure in Figure 1A is that of an inactivated rather than an active complex.

For these reasons, the ¹⁵Nϵ and ¹⁵NϵH resonances of all six arginine residues in the NMR spectra of wild-type 4-OT were assigned, and the contributions to catalysis of the three active site arginines (Arg-11, -39, and -61) were determined by site-directed mutagenesis. Three mutants of 4-OT were constructed in which each arginine was replaced with an alanine (R11A, R39A, and R61A), removing both the charge and the steric bulk. A fourth mutant was also constructed in which Arg-39 was replaced with a glutamine (R39Q), thereby retaining some of the bulk and hydrogen-bonding capability of arginine. Finally, a double mutant was constructed in which both Arg-11 and Arg-39 were mutated to alanines (R11A/R39A). In this paper, the results from the kinetic, stereochemical, structural, and binding studies indicate that Arg-11 is important in both substrate binding and catalysis and Arg-39 contributes largely to catalysis, while Arg-61 plays little or no role in substrate binding or catalysis. In the following paper (*19*), the effects of mutations of the active

site arginine residues of 4-OT on the pK_a values of catalytic residues are reported.

EXPERIMENTAL PROCEDURES

Materials. All reagents, buffers, and solvents were obtained from either Aldrich Chemical Co. or Sigma Chemical Co. unless noted otherwise. Tryptone and yeast extract were obtained from Difco (Detroit, MI). The YM-3 ultrafiltration membranes and Centricon (10 000 MW cutoff) centrifugal microconcentrators were obtained from Amicon. Isopropyl-β-D-thiogalactoside (IPTG) and thin-walled PCR tubes were obtained from Ambion, Inc. (Austin, TX). The syntheses of 2-hydroxy-2,4-hexadienedioate (**2**) and 2-hydroxy-2,4-pentadienoate (**5**) (Scheme 1) have been described (*1, 3*). The construction of the plasmid pETOT which contains the gene for 4-OT under control of the T7 expression system (pET system, Novagen, Inc., Madison WI) has been described (*5*). The expression vector pET24a was obtained from Novagen, Inc. Restriction enzymes, T4 DNA ligase, low melting point agarose, the Magic PCR Preps DNA purification kit, and the Wizard Plus Minipreps DNA purification system were obtained from Promega Corp. (Madison, WI). The Geneclean II kit was purchased from Bio 101, Inc. (La Jolla, CA). Reagents for the PCR were obtained from either Gibco BRL (Gaithersburg, MD) or Perkin-Elmer (Norwalk, CT). Oligonucleotides for site-directed mutagenesis and DNA sequencing were synthesized by Oligos Etc. Inc. (Wilsonville, OR).

Strains. Escherichia coli strain JM109 was obtained from Promega Corp. and used for transformation of ligated plasmids. *E. coli* strain BL21(DE3)pLysS was obtained from Novagen and used for expression of the recombinant proteins. Cells for general cloning and expression were grown in LB media supplemented with kanamycin (Kn) (50−100 μg/mL). The composition of LB medium is described elsewhere (*20*).

General Methods. Techniques for restriction enzyme digestions, ligation, transformation, and other standard molecular biology manipulations were based on methods described elsewhere (*20*). DNA sequencing was done at the University of Texas (Austin) Sequencing Facility on a Perkin-Elmer/ABI Prism 377 DNA sequencer according to the instructions provided with the ABI Prism Dye-Terminator kit. The base sequence is determined by analyzing fluorescent dye-labeled nucleotide fragments. Kinetic data were obtained on a Hewlett-Packard 8452A Diode Array spectrophotometer. Enzyme activity was monitored by following the formation of **3** at 236 nm (*1*). The cuvettes were mixed by a stir/add cuvette mixer. The kinetic data were fitted by nonlinear regression data analysis using the Grafit program (Erithacus Software Ltd., Staines, U.K.) obtained from Sigma Chemical Co. HPLC was performed on a Waters system using either a Bio-Gel Phenyl 5-PW hydrophobic column, a Waters Protein Pak (DEAE-5PW) anion-exchange column, or a Pharmacia Superose 12 (HR 10/30) gel filtration column. Protein was analyzed by tricine−sodium dodecyl sulfate−polyacrylamide gel electrophoresis under denaturing conditions on 16% gels on a vertical gel electrophoresis apparatus obtained from Gibco (*21*). Trichloroacetic acid was used instead of acetic acid in the staining and destaining solutions. The concentrations of wild-type and mutant forms of 4-OT (in micrograms per milliliter) were determined from the

difference in absorption measurements at 215 and 225 nm multiplied by the factor 144 (*5, 22*). Routine ^{1}H NMR spectra were obtained with either a Bruker AM-250 or a Varian Unity INOVA-500 spectrometer.

Site-Directed Mutagenesis. The four single mutants of 4-OT (R11A, R39A, R39Q, and R61A) were prepared using the gene for 4-OT in the plasmid pETOT as the template (*5*). The gene is flanked by an *Nde*I restriction site and a *Sal*I restriction site. The double mutant of 4-OT (R11A/R39A) was prepared using the R11A-4-OT gene as the template. Mutations were made using the overlap extension polymerase chain reaction as described elsewhere (*23*). For the R11A, R39A, R39Q, and R11A/R39A mutants, the external PCR primers were oligonucleotides 5′-GATCTC-GATCCCGCGAAATAAATACG-3′ (designated primer A) and 5′-CAGTGGTGGTGGTGGTGGTG-3′ (designated primer D). Primer A corresponds to the coding sequence of a region of the pET-24a(+) vector ∼100 bp upstream from the *Nde*I restriction site while primer D corresponds to the complementary sequence of the His·Tag region of the pET-24a(+) vector. For the R61A mutant, the oligonucleotide 5′-GCAGCCAACTCAGCTTCC-3′ was used as primer D. This primer corresponds to the complementary sequence of the region ∼45 bp downstream from the His·Tag region of the pET-24a(+) vector. For the R11A mutant, the internal PCR primers were oligonucleotides 5′-CGTCGCTGGCGCCT-TCAAGG-3′ (primer B) and 5′-CCTTGAAGGCGCCAGC-GACG-3′ (primer C). For the R39A mutant and the R11A/R39A double mutant, the internal PCR primers were oligonucleotides 5′-GATAATCACGGCCACGCTGG-3′ (primer B) and 5′-CCAGCGTGGCCGTGATTATC-3′ (primer C). For the R39Q mutant, the internal PCR primers were oligonucleotides 5′-GTGATAATCACCTGCACGCTGGT-3′ (primer B) and 5′-ACCAGCGTGCAGGTGATTAT-CAC-3′ (primer C). For the R61A mutant, the internal PCR primers were oligonucleotides 5′-GACTCAGCGTGCCAC-CTTGCT-3′ (primer B) and 5′-AGCAAGCTCGCACGCT-GAGTC-3′ (primer C). In each set of primers, primer C contains the codon for the desired mutant (underlined) while the remaining bases correspond to the coding sequence of the 4-OT gene. Primer B is the complementary primer with the desired codon underlined. The PCR was carried out in a Perkin-Elmer DNA thermocycler 480 using template DNA, synthetic primers, and the PCR reagents supplied in either the PCR reagent system or in the Perkin-Elmer Cetus GeneAMP kit following a protocol described elsewhere (*10*). The template DNA was prepared using the Wizard Plus Minipreps DNA purification system as described (*10*). The AB and CD fragments were generated in separate PCRs as described (*10*). Subsequently, the mutated DNA fragment was produced by performing the PCR on a mixture of the AB and CD fragments (5 μL each) using primers A and D. The mutated DNA fragment and the pET24a(+) vector were digested with *Nde*I and *Sal*I restriction enzymes, purified, and ligated using T4 DNA ligase following a previously described protocol (*10*). Aliquots of the resulting mixture were transformed into competent *E. coli* JM109 cells and grown on LB/Kn (100 μg/mL) plates at 37 °C. Single colonies were chosen at random and grown in liquid LB/Kn media (50−100 μg/mL). The newly constructed plasmid was isolated and sequenced in order to verify the mutation. Subsequently, the mutated plasmid was transformed as

Scheme 3
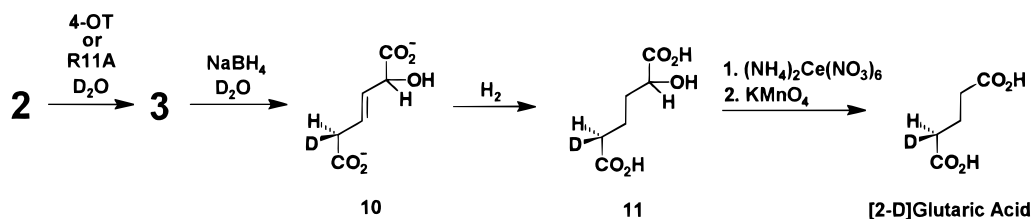
described elsewhere into *E. coli* strain BL21(DE3)pLysS for protein expression (*10*).

Overexpression and Purification of Recombinant Enzymes. A single colony of the expression strain containing the desired plasmid was used to inoculate 25 mL of LB/Kn medium (50–100 μg/mL). After overnight growth at 37 °C, 3 mL of the culture was used to inoculate 500 mL of LB/Kn medium (50–100 μg/mL) in a 2 L Erlenmeyer flask. Cultures were grown to an OD_{600nm} of ~0.6 at 37 °C with vigorous shaking and then induced with IPTG (1 mM final concentration). Incubation was continued for 4 h at 37 °C. Cells were harvested by centrifugation (7000g, 12 min) and stored at −80 °C. Typically, 2 L of culture grown under these conditions yields 7–8 g of cells.

4-Oxalocrotonate tautomerase and the mutant enzymes (R11A, R39A, R39Q, R61A) were purified to homogeneity using a published procedure (*10*). Typically, the yield of highly purified enzyme (>95% pure as assessed by SDS–PAGE) per liter is ~22 mg of R11A, ~78 mg of R39A, ~38 mg of R39Q, and 90 mg of R61A. The native molecular mass of each mutant was estimated by size exclusion chromatography on a Superose 12 column. Each of these mutant enzymes was chromatographed in 100 μL portions (~3–5 mg/mL) on the gel filtration column equilibrated with 20 mM sodium phosphate buffer, pH 7.3, at a flow rate of 0.2 mL/min. Protein was monitored at 254 nm. The wild type and the mutants eluted at ~80 min.

It was not possible to purify the R11A/R39A double mutant using the published procedure because the protein could not be recovered after passage through the hydrophobic column. Hence, the protein was partially purified on a DEAE anion-exchange column as follows. The crude cell lysate was centrifuged (15000g, 40 min), and the supernatant was injected in two portions (8 mL each) onto the DEAE anion-exchange column (15 × 2.15 cm) that had been equilibrated with 20 mM Tris-HCl buffer containing 20 mM NaCl, pH 7.4, at a flow rate of 5 mL/min. After a 10 min wash with the same buffer, the protein was eluted using a linear gradient (20–500 mM NaCl) over 50 min. The protein eluted after ~26 min. The yield of the partially purified enzyme (~75% pure) was ~38 mg/L of culture. The partially purified double mutant was chromatographed on a Superose 12 column as described above. The major peak eluted at ~80 min, comparable to wild-type 4-OT.

15N Labeling of R11A- and R39Q-4-OT. The uniformly ^{15}N-labeled R11A and R39Q 4-OT mutants were prepared in a MOPS-buffered medium by a protocol described elsewhere (*5*). The yield of purified enzyme (>95% as assessed by SDS–PAGE) per liter of culture is ~40 mg of ^{15}N wild-type 4-OT (*5*), ~16 mg of [15]N R11A, and ~14 mg of [15]N R39Q.

*Circular Dichroism Spectroscopy.* Circular dichroism

spectra of the wild-type enzyme, the four purified mutants, and the partially purified double mutant were measured in 20 mM sodium phosphate buffer (pH 7.3) at a concentration of approximately 10 μM in a CD cell with a 1.0 mm optical path length using a Jasco J-600 spectropolarimeter equipped with an IBM Personal System II computer (model 55-SX).

Mass Spectrometry. The monomeric masses of the purified mutant enzymes were determined by electrospray ionization mass spectrometry (ESI-MS) using a LCQ Finnigan octapole electrospray mass spectrometer. Samples for ESI-MS were analyzed in a solution of 80% (v/v) acetonitrile in water containing 0.05% TFA. Each sample was desalted on a Waters HPLC system using an Econosil C18 reverse-phase HPLC column (250 × 22 mm) in 500 μL portions (1–5 mg/mL) washing first with 0.05% TFA in water for 10 min and eluting with a linear gradient (0–100% acetonitrile/0.05% aqueous TFA) over the next 45 min at a flow rate of 5 mL/min. The effluent was monitored at 214 nm, and the major peaks were collected and analyzed by ESI-MS as described above. Typically, each mutant enzyme elutes as a single peak ~45 min after the injection.

4-OT- and R11A-4-OT-Catalyzed Ketonization of 2 to [5-D]3 in D$_2$O and Chemical Conversion to [2-D]Glutaric Acid. The stereochemical analysis of [5-D]**3**, generated by either 4-OT- or R11A-catalyzed ketonization of **2** in D$_2$O (Scheme 3), was performed by a modification of a published procedure (*24*). The stereochemistry of the 4-OT-catalyzed reaction was reinvestigated as a control. Each reaction mixture consisted of enzyme (4-OT, 0.3 μg; R11A, 60 μg) and **2** (4 mg) dissolved in DMSO-d_6 (30 μL). Sixteen reactions were carried out for each enzyme. All reactions were carried out in 100 mM Na$_2$DPO$_4$ in D$_2$O (0.6 mL, pD 9.3). The addition of **2** lowered the pD to ~6.8. The individual reaction mixtures were allowed to run at room temperature for either 2 min (4-OT) or 4 min (R11A), quenched with excess NaBH$_4$ (~40 μL of a 200 mg/mL solution in 100 mM Na$_2$DPO$_4$, pD 9.3, in D$_2$O), pooled, and purified by anion-exchange chromatography using a Dowex-1 (formate) column. The product 2-hydroxy-[5-D]-3-hexenedioate (**10**, Scheme 3) was eluted using a linear gradient of aqueous formic acid (0–4 M, 200 mL total). The product eluted between 2.5 and 3 M formic acid.

The saturated compound 2-hydroxy-[5-D]hexanedioate (**11**, Scheme 3) was obtained by catalytic hydrogenation of [5-D]**10** (45 mg for wild-type 4-OT and 47 mg for R11A) in a solution containing ethanol (5 mL), benzene (15 mL), and Wilkinson's catalyst (40 mg) as described (*24*). After the mixture had been shaken vigorously for 5 days under H$_2$ (55 psi), the product was isolated from both reactions by anion-exchange chromatography as described above to yield 12 mg (26% yield). The product eluted between 1.7 and 2 M formic acid.

Scheme 4
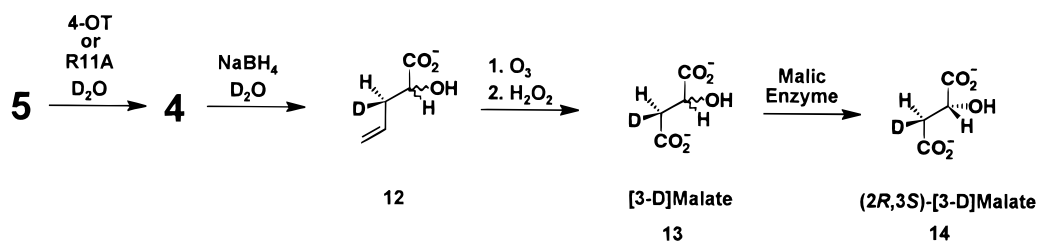
To convert [5-D]**11** to [2-D]glutaric acid, [5-D]**11** was dissolved in 1 M HNO_3 (2 mL), set stirring, and treated with a solution of ceric ammonium nitrate in 1 M HNO_3 (0.1 g/mL) which was added dropwise until a yellow color persisted. The reaction mixture was stirred for 1 h, and ceric ammonium nitrate was added as necessary in order to maintain the yellow color. Subsequently, a solution of potassium permanganate (26 mg/mL in concentrated HNO_3) was added dropwise to the reaction mixture until a purple color persisted. After the solution was allowed to stir for an additional hour (adding potassium permanganate as necessary), a solution of 5% sodium bisulfite was added dropwise until the solution became clear. The pH of the mixture was then adjusted to 9 by dropwise addition of 5 M NaOH. After filtration of the mixture through a 0.2 μm syringe filter, the [2-D]glutaric acid was isolated and purified by anion-exchange chromatography using a Dowex-1 (formate) column as described above. The product eluted between 1.5 and 1.8 M formic acid. A ^{1}H NMR spectrum obtained at 250 MHz corresponded to the previously reported spectrum (*24*). High-resolution mass spectrometry (HRMS) (*m/z* calculated for [2-D]glutaric acid $C_5H_7DO_4$ (MH$^+$) derived from the 4-OT reaction 134.0564), found 134.0566. HRMS (*m/z* calculated for [2-D]glutaric acid $C_5H_7DO_4$ (MH$^+$) derived from the R11A-4-OT reaction 134.0564), found 134.0562. Both samples of glutaric acid are contaminated with the di[2-D]glutaric acid. The sample derived from the 4-OT-catalyzed reaction contains 33% di[2-D]glutaric acid while the sample derived from the R11A-catalyzed reaction contains 43% di[2-D]glutaric acid. The molar ellipticities are corrected for the presence of the di[2-D]glutaric acid.

*R11A-4-OT-Catalyzed Ketonization of **5** to [3-D]**4** in D_2O and Chemical and Enzymatic Conversion to [3-D]Malate.* The stereochemical analysis of [3-D]**4**, generated by either wild-type 4-OT- or R11A-catalyzed ketonization of **5** in D_2O, was performed by a modification of a literature procedure (Scheme 4) (*3*). The stereochemistry of the 4-OT-catalyzed reaction was reinvestigated as a control. Each reaction mixture consisted of enzyme (4-OT, 1.4 μg; R11A, 23 μg) and **5** (4 mg) dissolved in DMSO-d_6 (30 μL). Individual reactions (24 for 4-OT and 27 for R11A) were carried out in 100 mM Na_2DPO_4 (0.6 mL, pD 9.3 in D_2O). The addition of **5** lowered the pD to $\sim$6.8. The individual reaction mixtures were allowed to run at room temperature for either 2 min (4-OT) or 4 min (R11A). Subsequently, they were quenched with excess $NaBH_4$ as follows and pooled. The 4-OT-catalyzed reactions were quenched with 3−10 μL portions of a 300 mg/mL solution of $NaBH_4$ in 100 mM Na_2DPO_4 in D_2O at 30 s intervals. The R11A-catalyzed reactions were quenched with a single 40 μL addition of a 200 mg/mL solution of $NaBH_4$ in 100 mM Na_2DPO_4 in D_2O. After the pH of the mixture was adjusted to 8, the mixture

was subjected to anion-exchange chromatography on a Dowex-1 (formate) column. The product, 2-hydroxy-[3-D]-4-pentenoate (**12**, Scheme 4), was eluted using a linear gradient of aqueous formic acid (0−2 M, 200 mL total). The product (24 mg) eluted between 0.75 and 0.9 M formic acid.

To convert **12** to [3-D]-D,L-malate (**13**), a solution of **12** in methanol (0.5 mL) and methylene chloride (10 mL) at −78 °C was subjected to a stream of O_3 until the solution turned blue ($\sim$15 min). Subsequently, the mixture was purged with O_2 until the blue color disappeared. After most of the solvent was removed, acetic acid (2 mL) and a 30% solution of hydrogen peroxide (0.6 mL) were added. After being stirred at room temperature overnight, the solution was concentrated by rotary evaporation. (HAZARD: Do not remove all solvent.) The concentrate was dissolved in 100 mM sodium phosphate buffer (pH 8) and treated with catalase (30 μL of a 2.4 mg/mL solution). The diastereomeric [3-D]-D,L-malate (10 mg) was purified by anion-exchange chromatography as described elsewhere (*3*). To remove the 2S isomer of [3-D]malate, the mixture was treated with malic enzyme and NADP$^+$ and purified by anion-exchange chromatography as described (*3*) to afford 1.6 mg (from 4-OT) or 1.7 mg (from R11A) of the 2R isomer of [3-D]malate (Scheme 4). (2R,3S)-[3-D]Malate (**14**) (from the R11A-catalyzed reaction): ^{1}H NMR (20 mM NaD_2PO_4 buffer in D_2O, pD 6.2, 500 MHz) δ 2.29 ($\sim$0.83 H, br d, $J_{2,3}$ = 10.0 Hz, H3), 4.22 ($\sim$0.83 H, br d, $J_{2,3}$ = 10.0 Hz, H2). (2R,3R)-[3-D]Malate (Scheme 4): δ 2.58 ($\sim$0.17 H, br s, H3), 4.20 ($\sim$0.17 H, br s, H2).

Structural NMR Methods. Unless otherwise stated, solution conditions for NMR studies of the enzyme were 3.0 mM (in subunits) uniformly ^{15}N-labeled wild-type 4-OT, the R11A mutant, or the R39Q mutant, and 8 mM sodium phosphate buffer, pH 6.5, in 0.6 mL of H_2O/D_2O (90:10) at 42 °C. The NMR data were collected on a Varian Unity Plus 600 NMR spectrometer equipped with z-axis pulsed field gradient capabilities, using a Varian 5 mm triple resonance probe. Data were processed on a Silicon Graphics Indigo 2 workstation using the FELIX software package (Biosym Technologies, Inc.). Multidimensional data sets were collected using the States−TPPI method (*25*) in all of the indirect dimensions, with relaxation delays of 0.9 s. These acquired domain data points were extended by one-third of the original size by the forward linear prediction routine in FELIX. Shifted (65° and 90°) sine bell filters were used in the first and subsequent dimensions, respectively, prior to zero-filling and Fourier transformation. The observed ^{1}H chemical shifts are referenced to the H_2O signal, which is 4.61 ppm downfield from external TSP at 42 °C and 4.89 ppm at 13 °C, and are reported with respect to TSP. The ^{15}N chemical shifts are measured with respect to external $^{15}NH_4Cl$ (2.9 mM in 1 M HCl) at 20 °C, which is 24.93

ppm downfield from liquid ammonia (*26*), and are reported with respect to liquid ammonia (*27*).

$^1H-^{15}N$ HSQC Spectra of R11A and R39Q Mutants. $^1H-^{15}N$ HSQC spectra were recorded on a 0.5 mM solution of either the ^{15}N-labeled R11A or R39Q mutant, 3.0 mM in subunits, containing the other components as described above, using a pulse sequence in which the HSQC detection scheme was optimized to avoid water saturation (*28*). The data were obtained at 600 MHz with spectral widths of 2000 and 8000 Hz in f_1 (^{15}N) and f_2 (^1H), respectively, and with 128 and 1024 complex points, respectively, in the t_1 and t_2 dimensions. A total of eight transients were acquired for each hypercomplex t_1 point with ^1H and ^{15}N carriers positioned at 4.61 and 120 ppm, respectively. The final data matrix was 512 × 512 real points for the f_1 (^{15}N) and f_2 (^1H) dimensions, respectively.

3D $^1H-^{15}N$ NOESY−HSQC of R11A and R39Q Mutants. 3D $^1H-^{15}N$ NOESY−HSQC experiments were recorded on the same samples with a 50 ms mixing time using the pulse sequence described (*29, 30*). The data were obtained at 600 MHz with spectral widths of 6400, 2000, and 8000 Hz in f_1 (^1H), f_2 (^{15}N), and f_3 (^1HN), respectively, with 128, 48, and 1,024 complex points, respectively, in the t_1, t_2, and t_3 dimensions. A total of 16 transients were acquired for each hypercomplex t_1, t_2 pair. The final data matrix was 256 × 128 × 256 real points for the f_1 (^1H), f_2 (^{15}N), and f_3 (^1HN), dimensions, respectively.

Selective $^1H-^{15}N$ HSQC Spectra of Arginine NεH. $^1H-^{15}N$ HSQC spectra selective for the side chain NεH of the arginine residues in wild-type 4-OT, the R11A mutant, and the R39Q mutant were recorded at 13 °C using the modified pulse sequence described (*31*) where the 180° ^{15}N pulse in the INEPT and the first 180° pulse in the refocused reversed INEPT portions were replaced by selective 180° pulses (340 μs). The data were obtained at 600 MHz with spectral widths of 730 and 8000 Hz in f_1 (^{15}N) and f_2 (^1H), respectively, and with 128 and 1024 complex points, respectively, in the t_1 and t_2 dimensions. A total of 8 transients were acquired for each hypercomplex t_1 point with ^1H and ^{15}N carriers positioned at 4.89 and 85 ppm, respectively. The final data matrix was 512 × 512 real points for the f_1 (^{15}N) and f_2 (^1H) dimensions, respectively.

Selective 2D NOESY−HSQC Spectra of Arginine NεH. 2D NOESY spectra selective for the side chain NεH of the arginine residues in wild-type 4-OT, the R11A mutant 4-OT, and the R39Q mutant 4-OT were recorded at 13 °C using the NOESY−HSQC pulse sequence where the $^1H-^{15}N$ HSQC portion is identical to the one described above. The data were obtained at 600 MHz with spectral widths of 730 and 8000 Hz in f_1 (^1H) and f_2 (^1H), respectively, and with 128 and 1024 complex points, respectively, in the t_1 and t_2 dimensions. A total of 16 transients were acquired for each hypercomplex t_1 point with ^1H and ^{15}N carriers positioned at 4.89 and 85 ppm, respectively. The final data matrix was 512 × 512 real points for the f_1 (^1H) and f_2 (^1H) dimensions, respectively.

$^1H-^{15}N$ HSQC Titration of R11A and R39Q Mutants with cis,cis-Muconate (8). Since the complex of the substrate analogue, *cis,cis*-muconate (**8**, CCM, Scheme 2), with both the R11A and R39Q mutants is in fast exchange on the chemical shift time scale (see Results and Discussion), the dissociation constant (K_d) and the amide ^{15}N and ^1H

assignments for the complex were determined by titration of the enzyme with CCM and following the changes in the ^1H and ^{15}N chemical shifts in a series of $^1H-^{15}N$ HSQC spectra obtained as described above. $^1H-^{15}N$ HSQC titrations of R11A and R39Q mutants, 2.0 mM in subunits, with CCM, were performed as described (*8*). The absolute values of the chemical shift changes ($\Delta\delta_{obs} = |\delta_o - \delta|$) for well-resolved resonances with significant $\Delta\delta_{max}$ values (L8, R39, and G51 of the R11A mutant; G51 and I52 of the R39Q mutant) were plotted against the total concentration of CCM (L_{tot}). Such plots were used to determine K_d according to eq 1, taking

$$\Delta\delta_{obs} = \Delta\delta_{max}[(K_d + L_{tot} + E_{tot}) - \sqrt{(K_d + L_{tot} + E_{tot})^2 - 4L_{tot}E_{tot}}]/2E_{tot} \quad (1)$$

into account the small changes in total enzyme subunit concentration, E_{tot}, due to dilution of the NMR sample upon addition of ligand, by performing nonlinear regression analysis using both L_{tot} and E_{tot} as codependent variables. As was found with the wild-type enzyme (*8*), a stoichiometry of one ligand binding site per subunit is assumed for this hexameric enzyme. The fractional occupancy of each binding site by CCM is obtained from the value of $\Delta\delta_{obs}/\Delta\delta_{max}$ calculated from eq 1 using the known values of K_d, L_{tot}, and E_{tot}.

The values of $\Delta\delta_{obs}$ for resonances which showed biphasic behavior (Q39 NεH$_a$ of the R39Q mutant) were plotted against the total concentration of CCM (L_{tot}), and such plots were used to determine the tight and weak dissociation constants, K_{d1} and K_{d2}, respectively, according to eqs 2 and 3. In eq 3 the concentration of tight binding sites (E_{tot1}) and

$$\Delta\delta_{obs} = \Delta\delta_{max}[(K_{d1} + L_{tot} + E_{tot1}) - \sqrt{(K_{d1} + L_{tot} + E_{tot1})^2 - 4L_{tot}E_{tot1}}]/2E_{tot1} + -\Delta\delta_{max}[(K_{d2} + L_{tot} + E_{tot2}) - \sqrt{(K_{d2} + L_{tot} + E_{tot2})^2 - 4L_{tot}E_{tot2}}]/2E_{tot2} \quad (2)$$

$$E_{tot1} = E_{tot2} = E_{tot}/2 \quad (3)$$

the concentration of weak binding sites (E_{tot2}) are assumed to be equal. This simplification is justified as follows. The biphasic nature of $\Delta\delta_{obs}$ for the Q39 NεH$_a$ resonance indicates two different modes of binding of CCM to the R39Q mutant, tight and weak. The binding of CCM solely to the active site in both modes is indicated by the observation that changes in backbone ^{15}N and NH chemical shifts were predominantly restricted to active site residues (see Results and Discussion). To model this behavior, eqs 2 and 3 arbitrarily assume that one-half of the total binding sites (three per hexamer) at a concentration of E_{tot1} exist with dissociation constant K_{d1} and that the other half of the total binding sites at a concentration of E_{tot2} exist with dissociation constant K_{d2}. Such half-site stoichiometry has previously been found in the inactivation of wild-type 4-OT by the affinity label 3-bromopyruvate (*5*). The dissociation constants did not change significantly for the monophasic titrations observed for L8, R39, and G51 of the R11A mutant as well as for G51 and I52 of the R39Q mutant when eq 1 was modified to assume half-site stoichiometry.

Table 1: Kinetic Parameters for 4-OT and Arginine Mutants[a]

enzyme	substrate	k_{cat} (s^{-1})	K_m (mM)	k_{cat}/K_m (M^{-1} s^{-1})	rel k_{cat}	rel K_m	rel k_{cat}/K_m
WT	2	3500 ± 500	0.18 ± 0.03	1.9×10^7	1.0	1.0	1.0
R11A	2	40 ± 6	1.6 ± 0.3	2.5×10^4	1.1×10^{-2}	8.6	1.3×10^{-3}
R39A	2	28 ± 2	0.29 ± 0.04	9.7×10^4	8.0×10^{-3}	1.6	5.1×10^{-3}
R39Q	2	9.0 ± 1	0.47 ± 0.07	1.9×10^4	2.6×10^{-3}	2.6	1.0×10^{-3}
R11A/R39A	2	≤0.4			≤10^{-4}		
R61A	2	3500 ± 240	0.29 ± 0.04	1.2×10^7	1.0	1.6	0.63
WT	5	0.40 ± 0.02	1.11 ± 0.10	3.6×10^2	1.0	1.0	1.0
R11A	5	1.0 ± 0.3	1.11 ± 0.33	9.0×10^2	2.5	1.0	2.5

[a] The steady-state kinetic parameters were determined at 23 °C and pH 7.3. Errors are standard deviations.

To determine the total concentration of CCM (L_{tot}) which maximized the occupancy of the tight site relative to the weak site in the R39Q mutant, the concentration of free CCM (L_f) was calculated at specific total concentrations of CCM (L_{tot}) from the cubic equation (eq 4) derived by assuming the

$$L_f^3 + (K_{d1} + E_{tot1} + K_{d2} + E_{tot2} - L_{tot})L_f^2 +$$
$$(K_{d1}K_{d2} + K_{d1}E_{tot2} + K_{d2}E_{tot1} - K_{d1}L_{tot} - K_{d2}L_{tot})L_f -$$
$$K_{d1}K_{d2}L_{tot} = 0 \quad (4)$$

simultaneous operation of both equilibria (*32*). In eq 4, K_{d1} and K_{d2} represent the dissociation constants of the tight and weak sites, respectively, and E_{tot1} and E_{tot2} represent the concentrations of the tight and weak sites, respectively. The concentration of CCM bound at the tight site (L_{b1}) is obtained from L_f, K_{d1}, and E_{tot1}, and the concentration of CCM bound at the weak site (L_{b2}) is obtained from L_f, K_{d2}, and E_{tot2}, by eqs 5 and 6, respectively. The fractional occupancies at the

$$L_{b1} = L_f E_{tot1}/(K_{d1} + L_f) \quad (5)$$

$$L_{b2} = L_f E_{tot2}/(K_{d2} + L_f) \quad (6)$$

tight and weak sites are L_{b1}/E_{tot1} and L_{b2}/E_{tot2}, respectively.

1D ^{15}N NMR Spectroscopy. 1D ^{15}N NMR experiments were performed at 42 °C on wild-type 4-OT, the R11A mutant, and the R39Q mutant. A Varian Unity-Plus 600 NMR spectrometer operating at 60.783 MHz for ^{15}N was used. Spectra were acquired without proton decoupling using a 5 mm broad-band detection probe. The ^{15}N chemical shifts were referenced to external liquid ammonia as described (*26, 27*). The acquisition parameters were as follows: spectral width, 12 001.2 Hz; acquisition time, 0.683 s; relaxation delay, 0.1 s; total number of transients, 10 000−100 000.

RESULTS AND DISCUSSION

Construction, Expression, and Characterization of the Mutants. The five mutants of 4-OT were constructed by overlap extension PCR, expressed in *E. coli* strain BL(DE3)-pLysS, and four mutants were purified to homogeneity (as assessed by SDS−PAGE) using previously described procedures (*10*). The sequence of each mutant was confirmed by DNA sequencing. The range of overproduction (per liter of culture) varied from 20 mg (R11A) to 90 mg (R61A). The R11A/R39A double mutant was partially (∼75%) purified using a DEAE anion-exchange column yielding ∼38 mg/L.

All of the mutants were analyzed by electrospray ionization mass spectrometry, gel filtration chromatography, and circular dichroism. Typically, each sample generates one major

peak that corresponds to the expected subunit molecular mass of each mutant (data not shown). In all cases, the amino-terminal proline is not blocked by the initiating methionine. It was further shown by size exclusion chromatography that the native molecular mass for each mutant is comparable to that of wild type. This result indicates that the mutants are hexamers in solution. Finally, the CD spectrum of each mutant was nearly identical to that recorded for wild type, indicating that the mutations did not result in any gross conformational changes (data not shown).

Kinetic Properties of R11A-, R39A-, R39Q-, R61A-, and R11A/R39A-4-OT. To examine the roles of Arg-11, Arg-39, and Arg-61, implicated in 4-OT catalysis by NMR and crystallographic studies (Figure 1) (*4, 8, 17*), the effects of mutating these residues on the kinetic parameters of 4-OT were studied (Table 1). Using the more reactive dicarboxylate substrate **2**, the R11A mutation decreased k_{cat} 88-fold and increased K_m 8.6-fold such that k_{cat}/K_m decreased 760-fold. With the less reactive monocarboxylate substrate **5**, the R11A mutation showed little or no effect on either k_{cat} or K_m compared to the same reaction catalyzed by the wild-type enzyme. Interestingly, the high K_m of substrate **5** with the wild-type enzyme agrees with the K_m of substrate **2** with the R11A mutant enzyme. This observation, together with the insensitivity of both k_{cat} and K_m of **5** to the R11A mutation, supports a significant role of Arg-11 in binding the 6-carboxylate group of the substrate. The loss of this interaction both in the R11A·**2** complex and in the wild type· **5** complex also results in large decreases in k_{cat} of ∼10^2- and ∼10^4-fold, respectively. The 10^2-fold greater loss in activity on removing the C-6 carboxylate group of the substrate likely results from the loss of the inductive and resonance effects of the carboxylate in facilitating substrate deprotonation (*6, 33*).

Mutations of Arg-39 to Ala and Gln result in 125-fold and 389-fold decreases in k_{cat} with small effects on K_m, suggesting a predominantly catalytic role for Arg-39 (Table 1). Mutation of Arg-61 to Ala shows no significant effects on k_{cat} or K_m, arguing against a role for Arg-61 in either catalysis or substrate binding. The R11A/R39A double mutant showed no detectable catalysis, indicating a loss of at least 10^4-fold in activity, based on the sensitivity of the kinetic assay. A 10^4-fold decrease in k_{cat}, the expected result of the approximate additivity of the effects on k_{cat} of the two single mutations, would suggest independent functioning of Arg-11 and Arg-39 (*34*).

*Stereochemical Analysis of R11A-4-OT Using **2** and **5**.* The stereochemical course of the 4-OT-catalyzed reaction was assigned previously by demonstrating that the enzyme converts **2** to (5*S*)-[5-D]**3** (Scheme 3) and **5** to (3*R*)-[3-D]**4**
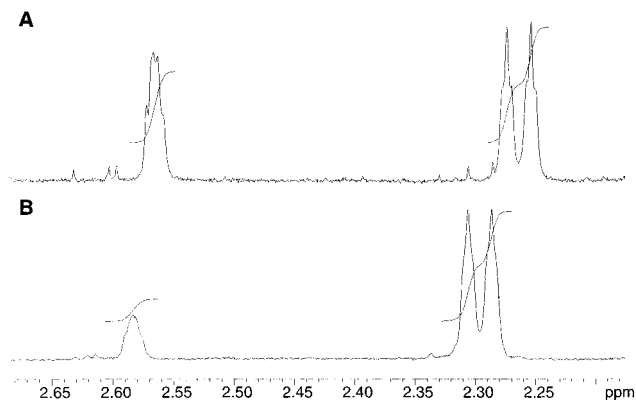
A

B

FIGURE 2: ^1H NMR spectra of (2R)-[3-D]malate obtained from chemical and enzymatic conversion of 2-oxo-[3-D]-4-pentenoate (**4**) generated by the (A) 4-OT-catalyzed ketonization of 2-hydroxy-2,4-pentadienoate (**5**) in D_2O and the (B) R11A-catalyzed ketonization of **5** in D_2O. In (A), the areas of the resonances at 2.56 and 2.26 ppm are 15 and 25 units, respectively. In (B), the areas of the resonances at 2.58 and 2.29 ppm are 6 and 30 units, respectively. Conditions: frequency, 500 MHz; 128 transients; recycle time, 6.8 s; flip angle, 20°; and $T = 27$ °C.

(Scheme 4). On the basis of these results, it was inferred that 4-OT catalyzes a suprafacial 1,3-allylic rearrangement of **1** to **3** (*3*). It was also noted that the enzyme-catalyzed ketonization of **2** to (5S)-[5-D]**3** is highly stereospecific (*24*) whereas the enzyme-catalyzed ketonization of **5** to (3R)-[3-D]**4** is only stereoselective (*3*). It was proposed that the interaction of the two carboxylate groups at C-1 and C-6 of **2** with active site residues anchors the substrate at the active site, which accounts for the observed stereospecificity in the ketonization of **2** to **3**. For the monocarboxylate substrate **5**, the missing 6-carboxylate group may permit the substrate to bind in two different orientations which leads to the

production of both stereoisomers (3R)-[3-D]**4** and (3S)-[3-D]**4** and accounts for the greatly diminished stereoselectivity in the ketonization of **5** to **4** (*24, 33*).

To examine this "anchoring hypothesis" further, the stereochemistry of the R11A mutant in both directions (**2** to **3** and **5** to **4**) was examined and compared to that of the reaction catalyzed by wild-type 4-OT which was reinvestigated as a control. The stereochemical analysis of the [5-D]-**3** was based on its chemical conversion to a monodeuterated glutaric acid using a modified version of a protocol reported elsewhere (Scheme 3) (*24*). It has previously been established that [2-D]glutaric acid obtained using this protocol with the wild-type 4-OT exhibits a positive Cotton effect in its circular dichroism spectrum with a molar ellipticity $[\theta]_{211} = +183°$ M^{-1} cm^{-1} without computer enhancement (*10, 24*). It was concluded from this result that the S-enantiomer of [5-D]**3** is generated (*10, 24*). The sample of purified [2-D]glutaric acid obtained for the wild-type 4-OT-catalyzed reaction, with increased sensitivity due to computer accumulation of the data, exhibited a positive Cotton effect in its circular dichroism spectrum with a molar ellipticity $[\theta]_{211} = +245°$ M^{-1} cm^{-1}, a result believed to be more accurate. The sample of purified [2-D]glutaric acid obtained for the R11A-catalyzed reaction also exhibited a positive Cotton effect in its circular dichroism spectrum but with a molar ellipticity $[\theta]_{211} = +90°$ M^{-1} cm^{-1}. From these values, it can be estimated that the 5S isomer is generated in approximately a 2.2:1 ratio by the R11A mutant whereas it is generated nearly exclusively by the wild-type enzyme (*24*).

The stereochemical analysis of the [3-D]**4** was based on its chemical and enzymatic conversion to a 2R-monodeu-terated malate using a modified version of a protocol reported elsewhere (Scheme 4) (*3*). Each diastereotopic proton at C-3
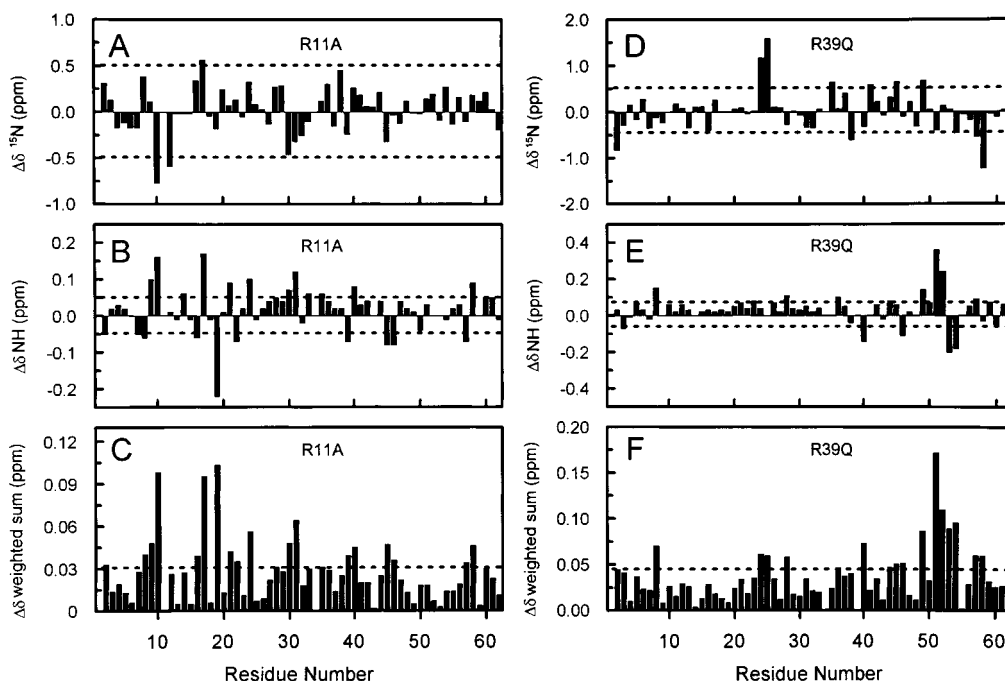

FIGURE 3: Backbone ^{15}N and NH chemical shift differences between wild-type 4-OT and either the R11A mutant (A–C) or the R39Q mutant (D–F) enzymes. Chemical shift differences ($\Delta\delta = \delta_{wild\ type} - \delta_{mutant}$) were calculated on the basis of the chemical shift values obtained from ^1H–^{15}N HSQC spectra (42 °C, pH 6.5) and plotted versus the residue number. (A, D) ^{15}N chemical shift differences. (B, E) NH chemical shift differences. (C, F) Sum of the absolute magnitudes of the ^{15}N and NH chemical shift changes which were weighted according to the backbone amide chemical shift dispersion in the ^{15}N and ^1H dimensions (27.16 and 2.11 ppm, respectively, for the R11A mutant; 27.36 and 2.28 ppm, respectively, for the R39Q mutant). The dashed lines indicate the error limit.
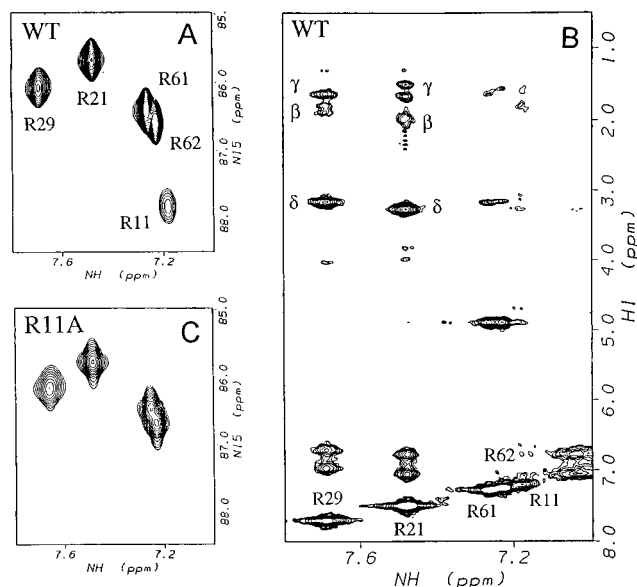
FIGURE 4: Assignment of the NεH resonances of arginine residues in 4-OT (13 °C, pH 6.5). (A) ¹H–¹⁵N HSQC spectrum selective for the side chain NεH of the arginine residues in wild-type 4-OT. (B) 2D NOESY spectrum selective for the side chain NεH of the arginine residues in wild-type 4-OT. (C) ¹H–¹⁵N HSQC spectrum selective for the side chain NεH of the arginine residues in the R11A mutant of 4-OT.

Table 2: ¹⁵N and ¹H Chemical Shift Values for the Side Chain ¹⁵Nε Nitrogen and NεH Proton Resonances of the Arginine Residues in Wild-Type 4-OT, Free and Complexed with CCM (**8**)[a]

residue	¹⁵Nε (ppm)[b]		¹⁵Nε (ppm)[c]		NεH (ppm)[c]	
	free	complex	free	complex	free	complex
Arg-11	88.35	88.30	87.83	87.30	7.18	7.84
Arg-21	86.46	86.41	85.68	85.68	7.48	7.47
Arg-29	86.84	86.93	86.09	86.00	7.69	7.70
Arg-39	85.51	86.70				
Arg-61	87.19	87.34	86.41	86.29	7.26	7.28
Arg-62	87.27	87.34	86.60	86.56	7.23	7.25

[a] Errors in ¹⁵Nε chemical shifts are ±0.5 ppm and in NεH are ±0.05 ppm. [b] 1D ¹⁵N NMR spectroscopy was performed at 42 °C and pH 9.7. [c] 2D selective ¹H–¹⁵N HSQC on arginine NεH was performed at 13 °C and pH 6.5.

of the fully protio malate appears as a doublet of doublets at 2.33 and 2.63 ppm (*35*). Stereospecific incorporation of a deuteron at C-3 results in the loss of one signal and the collapse of the remaining signal into a broadened doublet (*36*). The resonances for (2*R*)-[3-D]malate have been assigned by the reaction of maleic acid with maleate hydratase in D₂O (*35*). When the reaction is performed in D₂O, (2*R*,3*R*)-[3-D]malate is obtained (*35*). The resulting ¹H NMR spectrum shows the loss of an upfield signal (2.33 ppm) and the presence of a downfield doublet (2.66 ppm).

For the wild-type 4-OT-catalyzed conversion of **5** to **4** in D₂O, ¹H NMR analysis of the malate derived from [3-D]**4** by this procedure shows two signals, one signal is centered at 2.26 ppm and the other signal is centered at 2.56 ppm (Figure 2A). The integral of the signal at 2.26 ppm, assigned to the 2*R*,3*S* isomer, is ~1.7-fold greater than that of the corresponding integral for the 2*R*,3*R* isomer. Thus with the monocarboxylate substrate **5**, the wild-type 4-OT-catalyzed reaction is stereoselective with the 2*R*,3*S* isomer predominating by a ratio of only 1.7 to 1, in agreement with our previous observation (*3*). The stereochemistry at C-3 of [3-D]malate indicates that the stereochemistry at C-3 of **4** is *R*. The priority numbering at C-3 changes because there is a double bond instead of a carboxylate group at C-4 (Scheme 4).

For the R11A-catalyzed conversion of **5** to **4** in D₂O, ¹H NMR analysis of the malate derived from [3-D]**4** by this procedure shows the same signals centered at 2.29 and at 2.58 ppm (Figure 2B). However, the integral of the signal at 2.29 ppm, assigned to the 2*R*,3*S* isomer, is significantly greater (~5-fold) than that of the corresponding integral for the 2*R*,3*R* isomer. Again, the stereochemistry at C-3 of [3-D]malate assigns the stereochemistry at C-3 of **4** as *R*. Hence with the monocarboxylate substrate, the R11A-catalyzed reaction is 3-fold more stereoselective than the reaction catalyzed by wild-type 4-OT.

The results show that the stereoselectivity of the R11A-catalyzed reaction *decreases* when [5-D]**3** is generated from **2** but it *increases* when 3-[D]**4** is produced from **5** (in D₂O). The dicarboxylate substrate (at pD 6.8), inserting its negatively charged carboxylate group at C-6 into the relatively hydrophobic cavity of R11A where there is no longer a counterbalancing positive charge, may place the molecule in a "skewed" position such that Pro-1 can deliver a proton to either face of C-5. Such positioning may also be necessary to avoid any unfavorable interactions. As a result, a mixture of isomers is obtained. For substrate **5**, there is no negatively charged carboxylate group attached to C-5, possibly resulting in more precisely oriented binding of the terminal end of **5** in the hydrophobic pocket, favoring protonation on one face of **5** resulting in 3-fold greater stereoselectivity. Such oriented binding is presumably not possible in the wild-type enzyme because of the presence of Arg-11, resulting in lower stereospecificity.

Structural Properties of the R11A and R39Q Mutant Enzymes. It is important to determine whether loss of catalytic activity in a mutant enzyme is due to specific alteration of an important catalytic or substrate binding residue or to the loss of nativelike protein structure. As noted above, CD spectra of the R11A and R39Q mutants were indistinguishable from that of the wild-type enzyme, indicating that no gross conformational changes had occurred. The ¹H–¹⁵N HSQC spectrum of the R11A mutant enzyme indicates that 95% of the backbone ¹⁵N resonances are unshifted (i.e., are within the error limits of 0.5 ppm of those of the wild-type enzyme) and 68% of the backbone NH resonances are unshifted (i.e., are within the error limit of 0.05 ppm of those of the wild-type enzyme) (Figure 3A–C). Similar analysis of the R39Q mutant enzyme indicates that 84% of the backbone ¹⁵N resonances are unshifted and 61% of the backbone NH resonances are unshifted (Figure 3D–F). The backbone amide ¹⁵N and ¹H assignments for the R11A and R39Q mutants were confirmed by comparison of NOE cross-peaks to the backbone NH resonances, obtained by 3D ¹H–¹⁵N NOESY–HSQC spectra, to those of wild-type 4-OT in which complete ¹H,¹⁵N, and ¹³C chemical shift assignments have been made (*7*). ¹H–¹⁵N NOESY–HSQC spectra showed little change in NOE intensities for all residues, indicating very similar conformations for the wild-type and the R11A and R39Q mutant enzymes. While the overall three-dimensional fold is preserved in both the R11A and R39Q mutants, selective changes in ¹⁵N or NH chemical shifts in the ¹H–¹⁵N HSQC
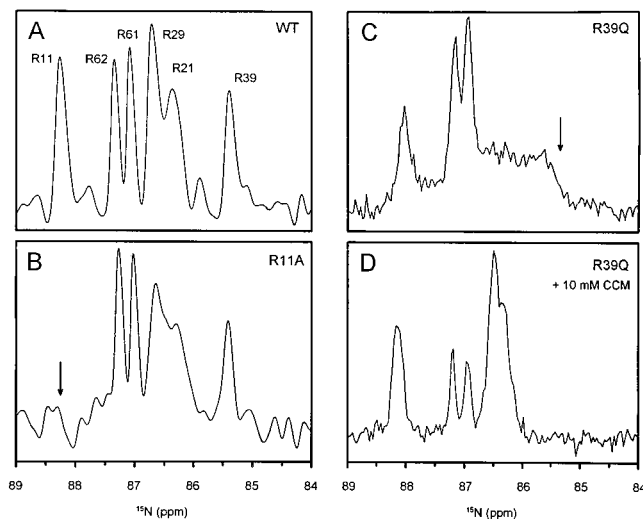
FIGURE 5: Upfield region of the 1D ^{15}N NMR spectrum (42 °C, pH 9.7) of (A) wild-type 4-OT, (B) the R11A mutant of 4-OT, (C) the R39Q mutant of 4-OT, and (D) the R39Q mutant of 4-OT in the presence of 10 mM CCM. The arrows shown in panels B and C indicate the chemical shift values for the side chain ^{15}Nϵ group of Arg-11 and Arg-39, respectively, in wild-type 4-OT.

spectrum were observed for Gly-10, Glu-17, Leu-19, and Leu-31 in the R11A mutant and for Gly-51, Ile-52, Gly-53, and Gly-54 in the R39Q mutant. X-ray (*4, 17*) and NMR studies (*7*) show that six of these eight residues are located near the active site and are in close proximity to the site of mutation. While Gly-10 is in the active site adjacent to Ala-11 in the R11A mutant, Glu-17 and Leu-19 are in the first half of the long helix from Asp-13 to Ser-30 which follows

position 11. All four of the residues showing changes in backbone ^{15}N and NH chemical shifts in the R39Q mutant are in the β-hairpin formed by residues 50–57 which overlies the active site.

Assignment of ^{15}Nϵ and NϵH Resonances of Arginine Residues in 4-OT. The availability of the arginine mutants facilitated the assignment of side chain ^{15}Nϵ and NϵH resonances of these residues. Figure 4A shows the ^{1}H–^{15}N HSQC spectrum selective for the side chain NϵH of the arginine residues in wild-type 4-OT. The assignments of the ^{1}H and ^{15}N chemical shifts for the NϵH group of four of the five resonances shown in Figure 4A (Arg-21, Arg-29, Arg-61, and Arg-62) (Table 2) were made on the basis of the correlation of each arginine NϵH proton chemical shift with the known chemical shifts of its side chain H$^\beta$, H$^\gamma$, and H$^\delta$ proton resonances (*7*) in the 2D NOESY spectrum selective for the side chain NϵH of the arginine residues in wild-type 4-OT (Figure 4B). The assignment of the ^{1}H and ^{15}N chemical shifts for the fifth resonance in Figure 4A to the NϵH group of Arg-11 (Table 2) was made on the basis of its disappearance in the selective ^{1}H–^{15}N HSQC spectrum of the R11A mutant of 4-OT (Figure 4C). This assignment was confirmed by the disappearance of the most downfield resonance in the directly detected 1D ^{15}N NMR spectrum of the R11A mutant (Figure 5A,B).

The cross-peak for the NϵH resonance of Arg-39 in wild-type 4-OT was not detectable in either the selective ^{1}H–^{15}N HSQC or the 2D NOESY spectra, suggesting that the NϵH proton is in fast exchange. However, the directly detected 1D ^{15}N NMR spectrum of wild-type 4-OT (Figure 5A) shows
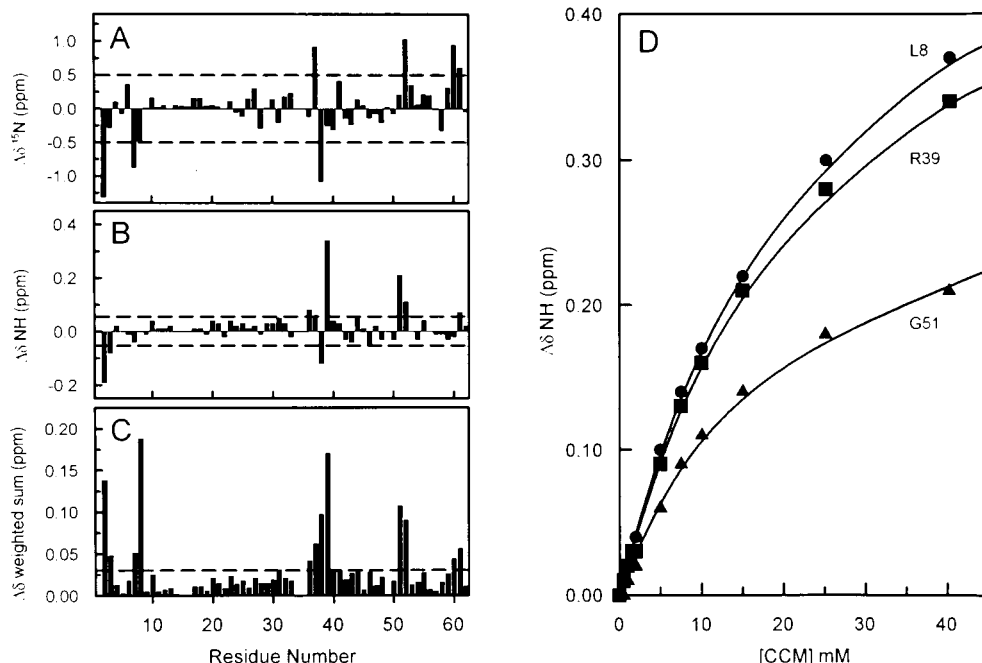

FIGURE 6: Changes in the backbone amide chemical shifts of the R11A mutant upon binding of CCM and determination of the dissociation constant for the complex (42 °C, pH 6.5). Chemical shift changes ($\Delta\delta = \delta_{\text{free enzyme}} - \delta_{\text{complex}}$) were calculated on the basis of the chemical shift values obtained from ^{1}H–^{15}N HSQC spectra and plotted versus the residue number of wild-type 4-OT. (A) ^{15}N chemical shift differences. (B) NH chemical shift differences. (C) Sum of the absolute magnitudes of the ^{15}N and NH chemical shift changes which were weighted according to the backbone amide chemical shift dispersion in the ^{15}N and ^{1}H dimensions (27.16 and 2.11 ppm, respectively). The dashed lines indicate the error limit. (D) The amide proton chemical shift changes of Leu-8 (●), Arg-39 (■), and Gly-51 (▲) were followed in a ^{1}H–^{15}N HSQC spectrum as the enzyme was titrated with CCM. The lines are described by eq 1 using dissociation constants of $K_d = 23.9 \pm 0.8$ mM (●), $K_d = 23.1 \pm 1.2$ mM (■), and $K_d = 18.0 \pm 1.8$ mM (▲) which yield a mean value of $K_d = 21.7 \pm 2.6$ mM for binding of CCM to the R11A mutant enzyme. From the dissociation constant for binding of CCM to the R11A mutant and eq 1, the occupancy is calculated to be 64% at the highest concentration of CCM (40 mM) in the titration used for the final ^{15}N and NH $\Delta\delta$ values in panels A–C.

Scheme 5

I   II   III
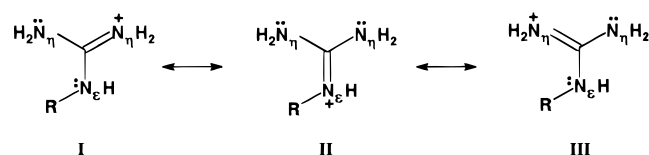
the presence of all six arginine $^{15}N\epsilon$ resonances enabling the ^{15}N chemical shift assignment of the most upfield resonance to the $N\epsilon$ of Arg-39 (Table 2). This assignment is confirmed by the disappearance of this upfield resonance in the R39Q mutant of 4-OT (Figure 5C). The broadening of the $N\epsilon$ resonances of Arg-21 and Arg-29 in the R39Q mutant, presumably due to exchange (Figure 5C), is reversed upon binding the intermediate analogue and competitive inhibitor CCM (Figure 5D). Although the arginine $^{15}N\epsilon$ and $N\epsilon H$ resonances were easily assignable, the $^{15}N\eta$ and $N\eta H_2$ resonances were not well resolved, and only those of Arg-29 were previously assigned (*7*).

1D ^{15}N NMR Titration of Wild-Type 4-OT with CCM (8). The binding of the intermediate analogue CCM (**8**) to wild-type 4-OT at 42 °C and pH 9.7 resulted in opposite changes in chemical shift of the $N\epsilon$ resonances of Arg-39 and Arg-11 (Table 2). The former shifted downfield by 1.19 ppm while the latter shifted upfield by 0.05 ppm. The upfield shift of Arg-11 induced by CCM binding was even greater (0.53 ppm) at 13 °C and pH 6.0. These differences in ^{15}N chemical shifts are consistent with differing modes of interaction of

Arg-39 and Arg-11 with carboxylate ligands. In the free enzyme, $N\epsilon$ of Arg-39 is the most shielded, resonating at 2.8 ppm upfield from Arg-11 $N\epsilon$ which is the least shielded (Table 2). A consideration of the three major resonance forms of the guanidinium side chain (Scheme 5) indicates that forms I and III contribute more than form II does to the structure of Arg-39, while the opposite is the case for Arg-11, with form II contributing more than forms I and III. Upon binding of CCM, Arg-39 $N\epsilon$ shifts downfield, indicating a greater contribution of resonance form II, relative to forms I and III, consistent with Arg-39 $N\epsilon H$ donating a hydrogen bond to an acceptor as in Figure 1. The small increase in chemical shift of Arg-11 $N\epsilon$ on CCM binding indicates a slightly decreased contribution of resonance form II relative to forms I and III, presumably as a result of hydrogen bond donation by the Arg-11 $N\eta H_2$ group(s) to an acceptor as in Figure 1B.

$^1H-^{15}N$ HSQC Titration of the R11A Mutant of 4-OT with CCM (8). As an independent test of the ability of the mutants to bind ligands at the active site, $^1H-^{15}N$ HSQC titrations were made of the R11A mutant with CCM, an analogue of the dienolic intermediate (**2**) in the 4-OT reaction. With wild-type 4-OT, CCM was previously found to be a linear competitive inhibitor with a K_i of 0.9 ± 0.2 mM (*8*). Titration of the wild-type enzyme with CCM, monitored by $^1H-^{15}N$ HSQC spectra, revealed changes in backbone ^{15}N and NH chemical shifts of residues near the active site, yielding a binding stoichiometry of 1.04 ± 0.06 per subunit and a K_d
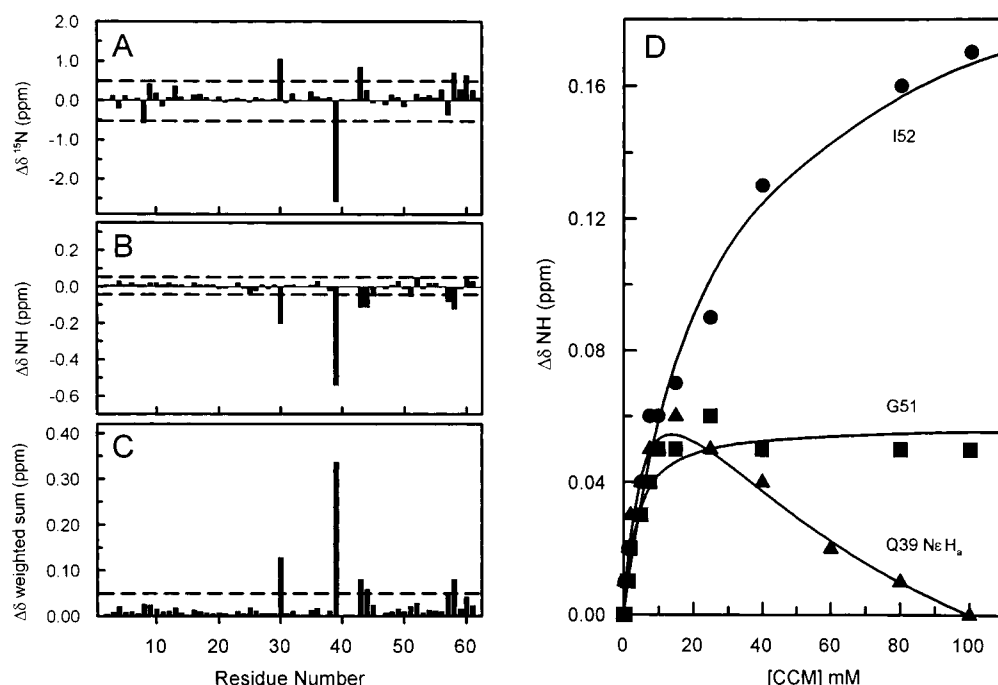

FIGURE 7: Changes in the backbone amide chemical shifts of the R39Q mutant upon binding of CCM and determination of the dissociation constant for the complex (42 °C, pH 6.5). Chemical shift changes ($\Delta\delta = \delta_{\text{free enzyme}} - \delta_{\text{complex}}$) were calculated on the basis of the chemical shift values obtained from $^1H-^{15}N$ HSQC spectra at 0 and 7.5 mM CCM and plotted versus the residue number of wild-type 4-OT. (A) ^{15}N chemical shift differences. (B) NH chemical shift differences. (C) Sum of the absolute magnitudes of the ^{15}N and NH chemical shift changes which were weighted according to the backbone amide chemical shift dispersion in the ^{15}N and ^1H dimensions (27.36 and 2.28 ppm, respectively). The dashed lines indicate the error limit. (D) The amide proton chemical shift changes of Ile-52 (●) and Gly-51 (■) were followed in a $^1H-^{15}N$ HSQC spectrum as the enzyme was titrated with CCM, and the curves are described by eq 1 using dissociation constants of $K_d = 24.5 \pm 3.2$ mM (●) and $K_d = 3.2 \pm 0.8$ mM (■) for binding of CCM to the R39A mutant enzyme. The side chain $N\epsilon H_a$ proton chemical shift changes of Gln-39 (▲) were biphasic and are fit by eqs 2 and 3 using dissociation constants of $K_{d1} = 6.0 \pm 1.7$ mM and $K_{d2} = 73 \pm 40$ mM. From the average K_d values for the tight sites (3.5 ± 1.6 mM) and the weak sites (29.3 ± 8.6 mM) and eqs 4–6, the occupancies at the tight sites and the weak sites are calculated to be 65% and 19%, respectively, at 7.5 mM CCM, which maximized the relative occupancy of tight and weak sites.

of 0.59 ± 0.14 mM, comparable to the K_i value (*8*).

With the R11A mutant, the ^{15}N and NH $\Delta\delta$ values ($= \delta_{free} - \delta_{complex}$) at the highest concentration of CCM used in the titration (40 mM) are plotted according to residue number in Figure 6A−C. Tracing the changes in chemical shifts of the amide resonances during the titration permitted the assignment of the ^{15}N−H amide cross-peaks of all 60 of the non-proline residues of the R11A mutant in the complex. Using eq 1 and the $\Delta\delta$(NH) values for Leu-8, Arg-39, and Gly-51, a K_d of 21.7 ± 2.6 mM for binding of CCM to the R11A mutant was determined (Figure 6D). This value is 37-fold higher than the K_d value for wild-type 4-OT (*8*), consistent with a major contribution of 2.3 kcal/mol by Arg-11 to CCM binding. Because of the weak binding of CCM to the R11A mutant, the binding stoichiometry could not be determined. Hence it was assumed to be 1.0 per active site as was found for the wild-type enzyme.

^1H−^{15}N HSQC Titration of the R39Q Mutant of 4-OT with CCM (8). The ^{15}N and NH $\Delta\delta$ values for the R39Q mutant at 7.5 mM CCM are plotted according to residue number in Figure 7A−C. In this titration, tracing the changes in chemical shifts of the amide resonances also permitted the assignment of the ^{15}N−H amide cross-peaks of all 60 of the non-proline residues of the R39Q mutant in the complex. In contrast to the wild-type enzyme (*8*), the P1G mutant (*10*), and the R11A mutant (Figure 6), all of which showed a single dissociation constant for CCM, the R39Q mutant of 4-OT shows two classes of binding sites for CCM, one with a tight dissociation constant and the other with a weak dissociation constant (Figure 7D). Using eq 1, a K_d of 3.2 ± 0.8 mM for binding of CCM to the tight sites was determined from the $\Delta\delta$(NH) values for Gly-51 (Figure 7D), and a K_d of 24.5 ± 3.2 mM for binding of CCM to the weak sites was determined from the $\Delta\delta$(NH) values for Ile-52 (Figure 7D).

In addition to the Gln-39 NϵH$_a$ and the Gly-51 NH proton resonances of the R39Q mutant (Figure 7D), tight binding of CCM was also observed for the backbone amide ^{15}N and NH chemical shifts of Met-45, Gln-39, and Ser-24 (Figure 8), yielding an overall average K_d of 3.5 ± 1.6 mM ($N = $ six resonances) for the tight site. In addition to the Gln-39 NϵH$_a$ and the Ile-52 NH proton resonances of the R39Q mutant (Figure 7D), weak binding of CCM was also observed for the backbone amide ^{15}N and NH chemical shifts of an additional nine residues (Figure 8), yielding an average K_d of 29.3 ± 8.6 mM ($N = 11$ resonances) for the weak sites, similar to the K_d of CCM from all sites of the R11A mutant. From these average dissociation constants for the binding of CCM to the tight and weak sites of the R39Q mutant, the concentration of CCM (7.5 mM) used for the final ^{15}N and NH $\Delta\delta$ values, given in Figure 7A−C, was selected on the basis that this concentration of CCM maximized the occupancy of the tight sites relative to the weak sites according to eqs 4−6.

Titration with CCM resulted in biphasic changes in chemical shift of the Gln-39 NϵH$_a$ resonance (Figure 7D). Hence values for $K_{d1} = 6.0 \pm 1.7$ mM and $K_{d2} = 73 \pm 40$ mM were determined for the binding of CCM to the tight and weak sites, respectively, by fitting the data to eqs 2 and 3. Although the errors are greater in fitting the biphasic titration, the K_d values overlap with those found in the monophasic titrations. The ^{15}N resonance of Met-45 also showed biphasic behavior. However, the changes in chemical
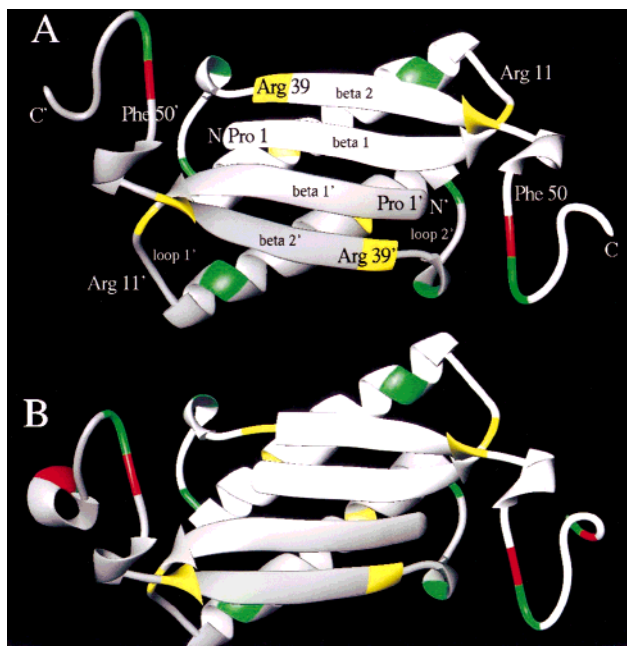

FIGURE 8: Tertiary structure of the 4-OT dimer unit in (A) the free enzyme and in (B) the enzyme, affinity-labeled with 2-oxo-3-pentynoate (*17*). Residues of R39Q that showed changes in backbone amide chemical shifts ($\Delta\delta$) upon binding of CCM are indicated. Those that showed tight binding ($K_d = 3.5 \pm 1.6$ mM) are marked in red. Those that showed weaker binding ($K_d = 29.3 \pm 8.6$ mM) are marked in green. Residues that showed both tight and weak binding are marked in yellow.

shift were too small to fit accurately, especially at the weak sites.

Figure 8 summarizes the regions of the X-ray structure (*17*) of the free enzyme (Figure 8A) and the enzyme covalently modified at the active site (Figure 8B), which show changes in ^{15}N and NH chemical shifts of R39Q associated with binding of CCM at tight sites (red), weak sites (green), and both tight and weak sites (yellow). The observation that both tight and weak modes of CCM binding affect predominantly active site residues argues against the nonspecific binding of CCM to remote sites on the protein and indicates site−site interaction with negative cooperativity among the six active sites of the R39Q mutant of 4-OT. Hence, a role for Arg-39 in substrate binding and catalysis, not only at proximal active sites but also at distant active sites in this hexameric enzyme, is also indicated. Such site−site interaction for Arg-39 is consistent with the X-ray crystal structure, which reveals that this residue comes from a different subunit to form the active site (Figure 1A) (*17*).

Magnitude of Acid Catalysis by 4-OT. The binding of CCM to wild-type 4-OT at -5.0 °C in 10% DMSO-d_6 did not induce the appearance of an additional cross-peak in the ^1H−^{15}N HSQC spectrum, assignable to Arg-39 NϵH, nor did (2*E*,4*E*)-2-fluoromuconate (2FM), a better analogue of the dienolic intermediate ($K_I \sim 45$ μM), consistent with Arg-39 NϵH remaining in fast exchange. Also, under these same conditions, no unusually deshielded proton resonances were detectable between 13 and 23 ppm in the complexes of wild-type 4-OT with either CCM, 2FM, or the equilibrium mixture of substrates, which consists of 8.2% **1**, 11.3% **2**, and 80.5% **3** free in solution (*1*). Hence these data provide no evidence for the participation of a short, strong (low-barrier) hydrogen bond in the mechanism of 4-OT, as was found in complexes
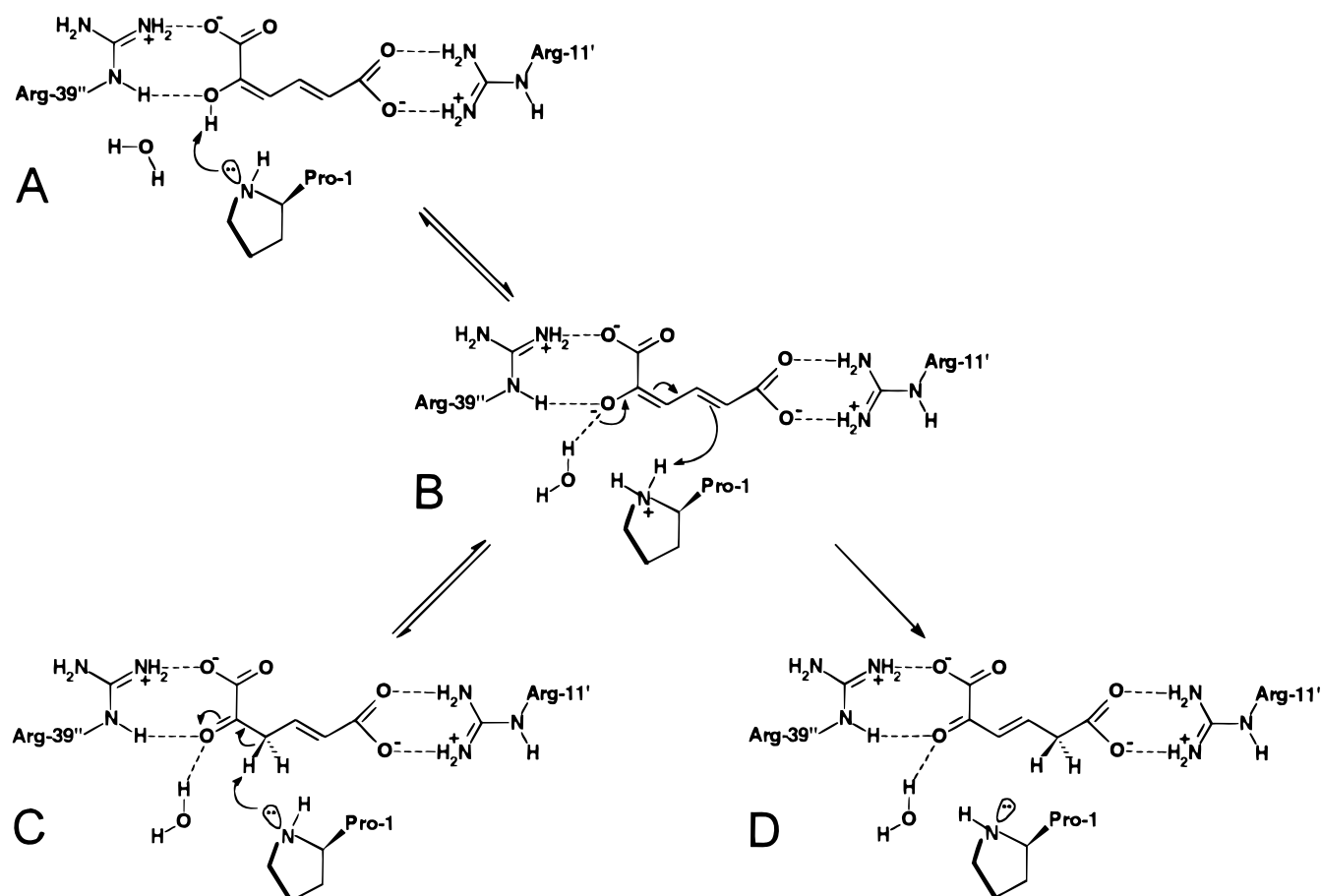
FIGURE 9: Reaction mechanism of 4-OT consistent with the mutational analysis of the roles of Arg-11 and Arg-39, as well as with previous kinetic (*5, 6*), mutagenesis (*9, 10*), and structural studies by X-ray crystallography (*4, 17*) and NMR spectroscopy (*7, 8*).

of ketosteroid isomerase (*14*) and triosephosphate isomerase (*13*) with intermediate analogues.

The absence of unusually strong hydrogen bonds and the modest acid catalysis in 4-OT, as reflected by the comparable effects on k_{cat} of mutations of Arg-11 and Arg-39 (Table 1), are not surprising. The dienolic intermediate **2** in the reaction catalyzed by 4-OT is more stable than the substrate **1**, indicating no thermodynamic barrier to substrate enolization (*1, 37*). With ketosteroid isomerase and triosephosphate isomerase, a significant contribution to rate enhancement results from lowering the large thermodynamic barriers to enolization of 11 kcal/mol (*38*) and 7.4 kcal/mol (*39*), respectively, requiring stronger acid catalysis than in 4-OT. Accordingly, the R39A and R39Q mutations of 4-OT decrease k_{cat} by factors of only $10^{2.1}$- and $10^{2.6}$-fold (Table 1), respectively, while mutation of the acid catalyst Tyr-14 to Phe in ketosteroid isomerase decreases k_{cat} by $10^{4.7}$-fold (*40*). In triosephosphate isomerase, mutation of the acid catalyst His-95 to Gln decreases the rate constant for enolization of glyceraldehyde 3-phosphate by $10^{3.6}$-fold and of dihydroxyacetone phosphate by $10^{2.6}$-fold (*11*). These values for triosephosphate isomerase are lower limits since another mechanism involving the general base, Glu-165, takes over in the H95Q mutant of this enzyme (*11−13*).

MECHANISTIC CONCLUSIONS

In the reaction catalyzed by 4-OT, the enzyme is presented with the dienol intermediate (**2**) which is more stable than the substrate (**1**). This raises the question of how 4-OT

obtains a proton to stereoselectively convert the dienol intermediate either to the substrate or to the product (**3**). The results of the present kinetic, stereochemical, structural, and binding studies, as well as the pH−rate profiles of the arginine mutants (*19*), are consistent with the mechanism in Figure 9 in which Arg-11 interacts with the 6-carboxylate of the substrate and Arg-39 interacts with the 1-carboxylate and the oxygen at C-2. The unusually low pK_a value of the general base Pro-1 (pK_a = 6.4) (*6, 19*) results in its being largely deprotonated under physiological conditions so that direct protonation of **2** to form **3** is unlikely. A reasonable mechanism is that Pro-1 initiates the reaction by deprotonating the 2-OH group of the dienol (Figure 9, A → B). This step would be facilitated by an increase in the pK_a of Pro-1 upon binding the dienol (*6, 41*) as found by direct ^{15}N titration of Pro-1 in the CCM complex of wild-type 4-OT (*19*). A similar mechanism has been proposed for the H95Q mutant of triosephosphate isomerase (*11*). Subsequently, Pro-1 rapidly and reversibly protonates the dienolate at C-3 to generate the unconjugated enone (B ⇌ C). In the rate-limiting step, defined by k_{cat}, Pro-1 protonates C-5 to yield the conjugated enone product (B → D).

Comparison of k_{cat} (3500 s^{-1}) with the pseudo-first-order rate constant for the nonenzymatic conversion of the dienolate to the conjugated enone product catalyzed by water and hydroxide under otherwise similar conditions (1.7 × 10^{-4} s^{-1}) (*1*) yields a rate acceleration or catalytic power for 4-OT of $10^{7.3}$-fold. From the effects of the R11A mutation on k_{cat}, Arg-11 contributes $10^{1.9}$-fold to the rate acceleration by

proper "anchoring" and orientation of the substrate and by inductive and resonance effects in the conversion of B → D. From the effects of the R39Q mutation, Arg-39, possibly assisted by an ordered water molecule, contributes $10^{2.6}$-fold to catalysis by facilitating the reversible polarization of the 2-keto group of the substrate in the C → B → D reactions. Arg-39 also stabilizes the β-hairpin which covers the active site. The 3-fold lower k_{cat} of the R39Q mutation compared to the R39A mutation may result from a greater perturbation of the β-hairpin by Gln-39 as reflected in the changes in backbone ^{15}N and NH chemical shifts and in the negative cooperativity in CCM binding and in the ionization of Pro-1 (*19*). Pro-1, functioning as the general base to mediate proton transfer between C-3 and C-5, contributes at least $10^{3.4}$-fold to catalysis as approximated by the reduction in k_{cat} of the P1L mutant which is unprocessed, hence blocked by methionine (*10*). A better estimate of $10^{4.9}$-fold for the contribution of Pro-1 to catalysis is provided by k_{cat} of the chemically synthesized and reconstituted 4-OT containing a cyclopentyl group in the first position (0.05 s^{-1}).[2] Simple additivity of the contributions of Arg-11, Arg-39, and Pro-1 to lowering the kinetic barrier to catalysis would yield a total effect of $10^{9.4}$, which exceeds the catalytic power of 4-OT, $10^{7.3}$, by a factor of $10^{2.1}$. Hence the individual effects of mutations on catalysis must be partially additive. It has previously been noted that partial additivity of catalytic effects reflects cooperativity among the catalytic residues (*34*). The approximate additivity of the effects of the R11A and R39A mutations in the R11A/R39A double mutant suggests that Arg-11 and Arg-39 act independently. Hence the likely effects which are cooperative involve Pro-1 interacting with one or both of the catalytic arginine residues, a point which is testable by appropriate double mutations.

It has been demonstrated that the 6-carboxylate group of substrate **2** is trans with respect to the extended carbon chain whereas the configuration of the 1-carboxylate group is unknown (*1*). If the interactions observed in the inactivated complex (Figure 1A) are used as a basis for modeling the interactions with the bound substrate (Figure 1B), then the 1-carboxylate group of substrate **2** would be cis with respect to the extended carbon chain as shown in Figure 9, permitting polarization of the substrate carbonyl group by the NϵH of Arg-39.

Although the X-ray structure of 4-OT inactivated by the active site-directed irreversible inhibitor **9** shows an interaction between the terminal carboxylate group of the inhibitor and the side chain guanidinium group of Arg-61 (Figure 1), Arg-61 does not play a significant role in the proposed mechanism on the basis of the unchanged kinetic parameters of the R61A mutant (Table 1). As pointed out elsewhere (*18*), protein X-ray crystallography is an insensitive technique for measuring hydrogen bond lengths. Alternatively, the interaction seen with the covalent inhibitor may not reflect the interaction of the substrate.

ACKNOWLEDGMENT

REFERENCES

1. Whitman, C. P., Aird, B. A., Gillespie, W. R., and Stolowich, N. J. (1991) *J. Am. Chem. Soc. 113*, 3154−3162.
2. Harayama, S., Rekik, M., Ngai K.-L., and Ornston, L. N. (1989) *J. Bacteriol. 171*, 6251−6258.
3. Lian, H., and Whitman, C. P. (1993) *J. Am. Chem. Soc. 115*, 7978−7984.
4. Subramanya, H. S., Roper, D. I., Dauter, Z., Dodson, E. J., Davies, G. J., Wilson, K. S., and Wigley, D. B. (1996) *Biochemistry 35*, 792−802.
5. Stivers, J. T., Abeygunawardana, C., Mildvan, A. S., Hajipour, G., Whitman, C. P., and Chen, L. H. (1996) *Biochemistry 35*, 803−813.
6. Stivers, J. T., Abeygunawardana, C., Mildvan, A. S., Hajipour, G., and Whitman, C. P. (1996) *Biochemistry 35*, 814−823.
7. Stivers, J. T., Abeygunawardana, C., Whitman, C. P., and Mildvan, A. S. (1996) *Protein Sci. 5*, 729−741.
8. Stivers, J. T., Abeygunawardana, C., Mildvan, A. S., and Whitman, C. P. (1996) *Biochemistry 35*, 16036−16047.
9. Fitzgerald, M. C., Chernushevich, I., Standing, K. G., Whitman, C. P., and Kent, S. B. H. (1996) *Proc. Natl. Acad. Sci. U.S.A. 93*, 6851−6856.
10. Czerwinski, R. M., Johnson, W. H., Jr., Whitman, C. P., Harris, T. K., Abeygunawardana, C., and Mildvan, A. S. (1997) *Biochemistry 36*, 14551−14560.
11. Nickbarg, E. B., Davenport, R. C., Petsko, G. A., and Knowles, J. R. (1988) *Biochemistry 27*, 5948−5960.
12. Harris, T. K., Cole, R. N., Comer, F. I., and Mildvan, A. S. (1998) *Biochemistry 37*, 16828−16838.
13. Harris, T. K., Abeygunawardana, C., and Mildvan, A. S. (1997) *Biochemistry 36*, 14661−14675.
14. Zhao, Q., Abeygunawardana, C., Gittis, A. G., and Mildvan, A. S. (1997) *Biochemistry 36*, 14616−14626.
15. Massiah, M. A., Abeygunawardana, C., Gittis, A. G., and Mildvan, A. S. (1998) *Biochemistry 37*, 14701−14712.
16. Wu, R. W., Ebrahemian, S., Zawrotney, M. E., Thornberg, L. D., Perez-Alverado, G. C., Brothers, G. C., Pollack, R. M., and Summers, M. F. (1997) *Science 276*, 415−418.
17. Taylor, A. B., Czerwinski, R. M., Johnson, W. H., Jr., Whitman, C. P., and Hackert, M. L. (1998) *Biochemistry 37*, 14692−14700.
18. Harris, T. K., and Mildvan, A. S. (1999) *Proteins: Struct., Funct., Genet. 35*, 275−282.
19. Czerwinski, R. M., Harris, T. K., Johnson, W. H., Jr., Legler, P. M., Stivers, J. T., Mildvan, A. S., and Whitman, C. P. (1999) *Biochemistry 38*, 12358−12366.
20. Sambrook, J., Fritsch, E. F., and Maniatis, T. (1989) *Molecular Cloning: A Laboratory Manual*, Cold Spring Harbor Laboratory, Cold Spring Harbor, NY.
21. Chen, L. H., Kenyon, G. L., Curtin, F., Harayama, S., Bembenek, M. E., Hajipour, G., and Whitman, C. P. (1992) *J. Biol. Chem. 267*, 17716−17721.
22. Waddell, W. J. (1956) *J. Lab. Clin. Med. 48*, 311−314.
23. Ho, S. N., Hunt, H. D., Horton, R. M., Pullen, J. K., and Pease, L. R. (1989) *Gene 77*, 51−59.
24. Whitman, C. P., Hajipour, G., Watson, R. J., Johnson, W. H., Jr., Bembenek, M. E., and Stolowich, N. J. (1992) *J. Am. Chem. Soc. 114*, 10104−10110.
25. Marion, D., Driscoll, P. C., Kay, L. E., Wingfield, P. T., Bax, A., Gronenborn, A. M., and Clore, G. M. (1989) *Biochemistry 28*, 6150−6156.
26. Levy, G. C., and Lichter, R. L. (1979) in *Nitrogen-15 NMR Spectroscopy*, John Wiley & Sons, Inc., New York.
27. Weber, D. J., Abeygunawardana, C., Bessman, M. J., and Mildvan, A. S. (1993) *Biochemistry 32*, 13081−13088.
28. Mori, S., Abeygunawardana, C., Johnson, M. O., and van Zijl, P. C. M. (1995) *J. Magn. Reson. 103B*, 203−216.
29. Zhao, Q., Abeygunawardana, C., and Mildvan, A. S. (1997) *Biochemistry 36*, 3458−3472.

---

[2] C. P. Whitman, M. C. Fitzgerald, and R. M. Czerwinski, unpublished observations, 1999.

30. Kay, L. E., Keifer, P., and Saarinen, T. (1992) *J. Am. Chem. Soc. 114*, 10663−10665.

31. Zhang, O., Kay, L. E., Olivier, P. J., and Forman-Kay, J. D. (1994) *J. Biomol. NMR 4*, 845−858.

32. Miziorko, H. M., and Mildvan, A. S. (1974) *J. Biol. Chem. 249*, 2743−2750.

33. Lian, H., Czerwinski, R. M., Stanley, T. M., Johnson, W. H., Jr., Watson, R. J., and Whitman, C. P. (1998) *Bioorg. Chem. 26*, 141−156.

34. Mildvan, A. S., Weber, D. J., and Kuliopulos, A. (1992) *Arch. Biochem. Biophys. 294*, 327−340.

35. Gawron, O., Glaid, A. J., and Fondy, T. P. (1961) *J. Am. Chem. Soc. 83*, 3634−3640.

36. Englard, S., Britten, J. S., and Listowsky, I. (1967) *J. Biol. Chem. 242*, 2255−2259.

37. Whitman, C. P. (1999) in *Comprehensive Natural Products Chemistry* (Barton, D., Nakanishi, K., and Meth-Cohn, O., Eds.) Vol. 5, pp 31−50, Elsevier Science Ltd., Oxford, U.K.

38. Hawkinson, D. C., Eames, T. C. M., and Pollack, R. M. (1991) *Biochemistry 30*, 10849−10858.

39. Richard, J. P. (1984) *J. Am. Chem. Soc. 106*, 4926−4936.

40. Kuliopulos, A., Mildvan, A. S., Shortle, D., and Talalay, P. (1989) *Biochemistry 28*, 149−159.

41. Richard, J. P. (1988) *Biochemistry 37*, 4305−4309.

BI991116E